

Statistical occurrence of mirror mode waves at Mars

Cyril Simon Wedlund⁽¹⁾, Martin Volwerk⁽¹⁾, Christian Mazelle⁽²⁾, Christian Möstl⁽¹⁾, Diana Rojas-Castillo^(1,3), Jared Espley⁽⁴⁾ and Jasper Halekas⁽⁵⁾

(1) Space Research Institute (IWF), Austrian Academy of Sciences, Graz, Austria (cyril.simon.wedlund@gmail.com), (2) Institut de Recherche en Astrophysique et Planétologie (IRAP), Toulouse, France
 (3) Universidad Nacional Autónoma de México, Facultad de Ciencias, México DF, Coyoacán, MX, (4) NASA Goddard Space Flight Center, Laboratory for Planetary Magnetospheres, Greenbelt, MD, USA
 (5) Department of Physics and Astronomy, University of Iowa, Iowa City, IA, US



1. Introduction

Ultra low-frequency wave activity such as mirror mode (MM) waves, arising from an ion temperature anisotropy in the plasma, has been ubiquitously detected in the magnetosheaths of Venus (e.g., Volwerk+ 2008) and Mars (e.g., Ruhunusiri+ 2015). The MM instability is typically triggered behind a quasi-perpendicular bow shock in a high plasma β . The instability grows when the following criterion is fulfilled in the plasma (Hasegawa 1969):

$$1 + \sum_i \beta_{i\perp} \left(1 - \frac{T_{i\perp}}{T_{i\parallel}} \right) < 0$$

where \parallel and \perp denote the directions parallel and perpendicular to the ambient magnetic field direction, and the sum is over all ion species i .

Mirror mode waves are low-frequency long-wavelength transverse waves, usually linearly polarised and non-propagating. They can be characterised in the data by sudden dips or peaks in the magnetic field intensity anti-correlated with plasma density variations. In Venus Express data, such structures may last from a few seconds up to about 30 s on average (Volwerk et al. 2016).

With MAVEN, because the orbit's period is much lower (about 4.5h compared to 24h), such structures are expected to appear on shorter timescales.

We present here a survey of detected mirror mode waves at Mars using magnetometer data from the NASA/MAVEN mission between 2014 and 2019 (solar cycle 24, receding activity). First, bow shock crossings are identified in the data using analytical models. MM waves are then automatically detected from magnetometer measurements only. Preliminary maps of MM wave occurrence for solar cycle 24 are presented and aimed at being compared with similar and different solar activity conditions with MGS and Mars Express data. Expected refinements and work in progress are discussed, especially with the use of the high-temporal resolution ion moment data from the ion analysers on MAVEN.

3. Bow shock and Mirror Mode detections

To detect MAVEN bow shock crossings and take into account the asymmetry around the X_{MSO} axis in aberrated Mars-centric Solar Orbital coordinates (Edberg+ 2008, Hall+ 2016, 2019), a simple geometric algorithm is used, based on the 3D parameterisation of Gruesbeck+ (2018). Their 3D quadratic Cartesian model is first re-expressed in spherical coordinates with two spherical angles (θ, ϕ) to describe MAVEN's orbit. Comparing MAVEN's planetocentric distance with that calculated by the quadratic bow shock model at the same angles (θ, ϕ) yields the approximate position of the bow shock. The algorithm is accurate within about 20 min (Fig. 2).

After filtering/minimum variance analysis (MVA), criteria for mirror mode detections (Soucek+ 2008, Volwerk+ 2016) are:

- Angle betw. maximum variance direction & that of the background field $\Theta < 20^\circ$ (linearly polarised waves)
- Angle betw. minimum variance direction & $\Phi > 80^\circ$ (idem)
- Fluctuations of the order of the mean field intensity $\Delta|B|/|B| < 0.1$ (compressional structure)
- Eigenvalues of the variance analysis so that $\lambda_{max}/\lambda_{int} > 1.5$ and $\lambda_{min}/\lambda_{int} > 0.3$ (MVA well defined)

A test case is shown in Fig. 2 (right), whereas selection criteria for 3 orbits on 01-11-2014 give different results in Table 1.

Criteria	Θ_{max}	Φ_{min}	$\Delta B / B $	$\lambda_{max}/\lambda_{int}$	# detections	Total duration (s)	Comments
I	X				682	13128	$\frac{\Delta B }{ B } \geq 0.1$
II	X	X			733	25476	$\frac{\Delta B }{ B } > 1.5, \frac{\lambda_{max}}{\lambda_{int}} > 0.3$
III	X	X	X		214	2356	$\Theta_{max} \leq 20^\circ, \Phi_{min} \geq 80^\circ$
IV	X	X	X	X	110	449	Soucek et al. (2008), $\Theta_{max} \leq 30^\circ, \frac{\lambda_{max}}{\lambda_{int}} \geq 0.25$
V	X	X	X	X	146	1281	Volwerk et al. (2016)
VI	X	X	X	X	96	660	Volwerk et al. (2016) + Soucek et al. (2008)

Table 1: Evolution of number of candidate detections with selection criteria. Two mirror events are separated by at least 10 s to be counted. Mixing the criteria of Soucek+ (2008) those of Volwerk+ (2016) are chosen in the following.

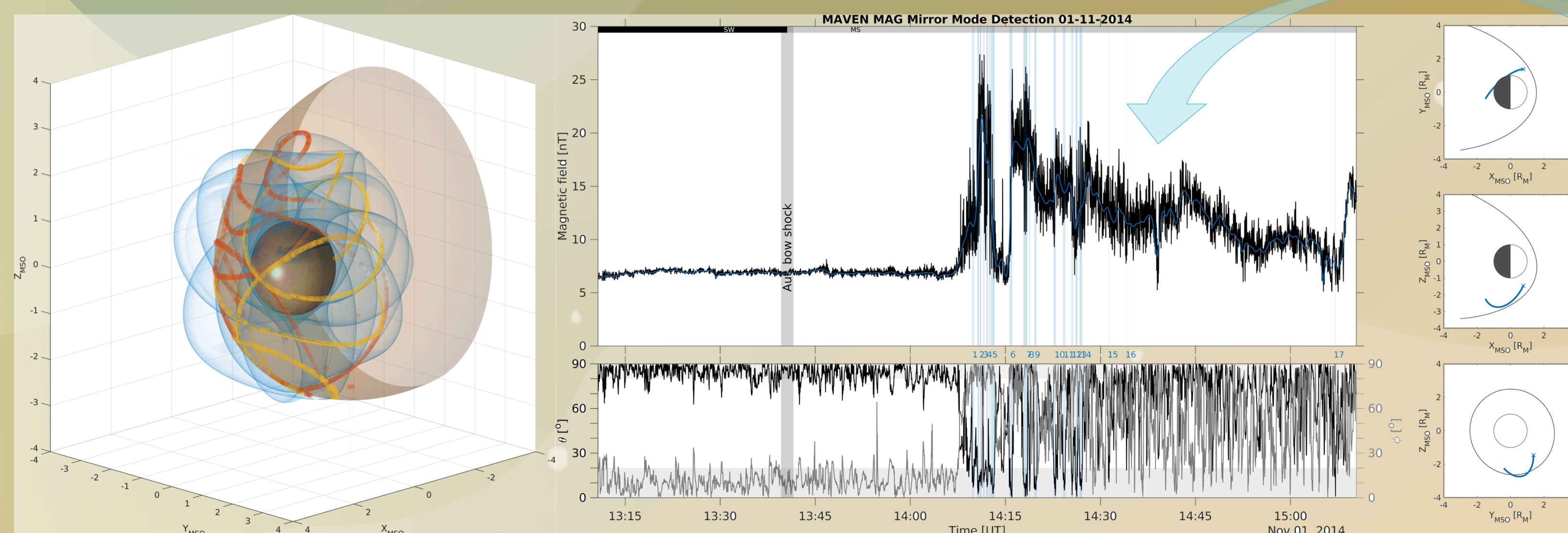


Fig. 2: Left: automatic detection of bow shock crossings. Right: MAG magnetic field (top panel) and angles to the maximum and minimum variance directions (bottom panel). Potential mirror mode detections are highlighted by vertical blue lines.

Note that many of these detections appear close to the actual bow shock, and will need to be investigated with the full mirror instability criterion before validation.

2. The MAVEN dataset

The Mars Atmosphere and Volatile Evolution (MAVEN) spacecraft has been orbiting Mars since October 2014. It carries a suite of Particles and Fields instruments, including two tri-axial fluxgate magnetometers (MAG, Connerney et al. 2015) and the Solar Wind Ion Analyzer (SWIA, Halekas et al. 2015), both with high temporal resolution. MAG's cadence goes up to 32 Hz whereas SWIA typically measures ion fluxes from which ion moments of the ambient plasma can be derived with a characteristic 4-s resolution. Because SWIA does not discriminate ions in mass M , the plasma composition must be assumed and errors of the order of \sqrt{M} are introduced in the moments, which can be partially lifted with the cross-calibration with the SupraThermal And Thermal Ion Composition analyzer (STATIC, McFadden et al. 2015). Calibrated data is available until the end of 2019 in the Planetary Data System (PDS) archive maintained at NASA.

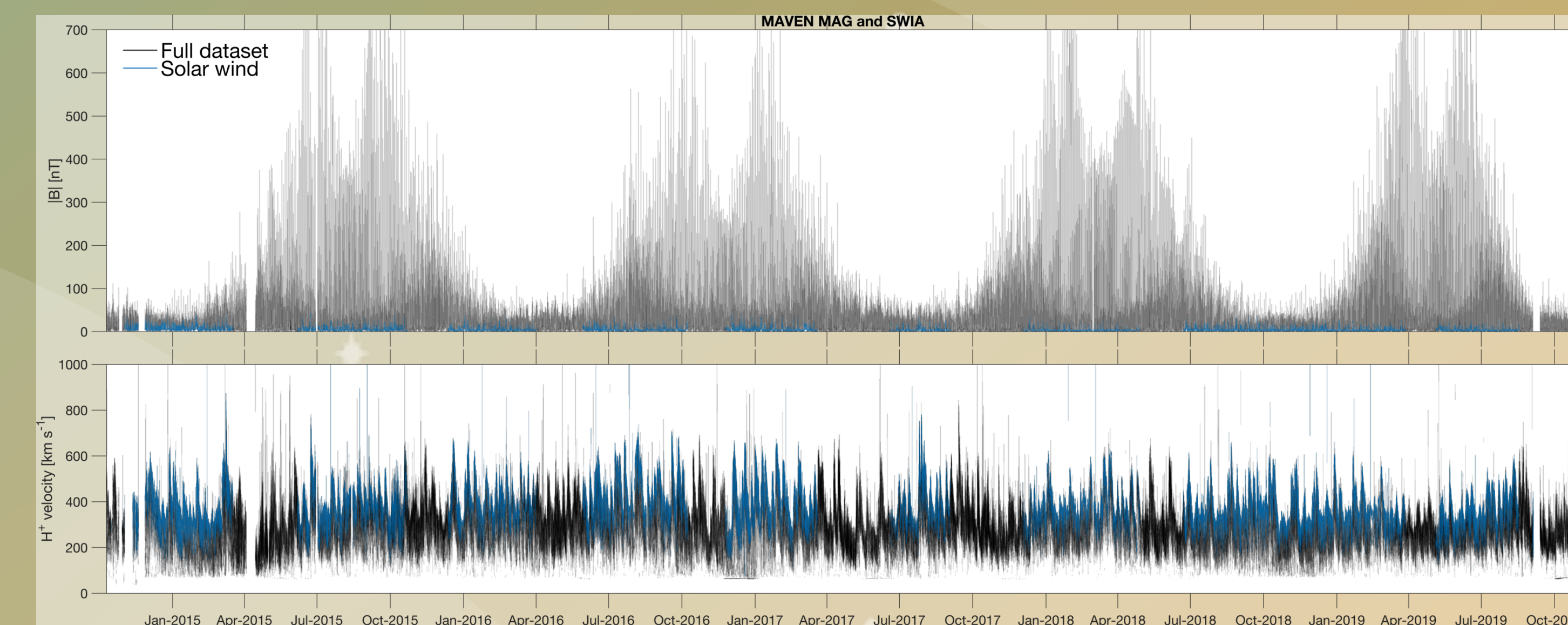


Fig. 1: MAVEN MAG magnetic field (top panel) and SWIA plasma velocity (bottom panel) 2014-2019. Filtered solar wind data are shown in blue in both panels.

Figure 1 shows a snapshot of the PDS-derived magnetic field intensity and proton velocity throughout the mission with a 1-min resolution. The magnetic field data exhibits a quasi-periodic behaviour, which is a combination of Mars' plasma environment and MAVEN's orbit. The solar wind data is shown in blue and results from the automatic detection of the bow shock, as sketched in Section 3.

4. Maps of Mirror Mode occurrence

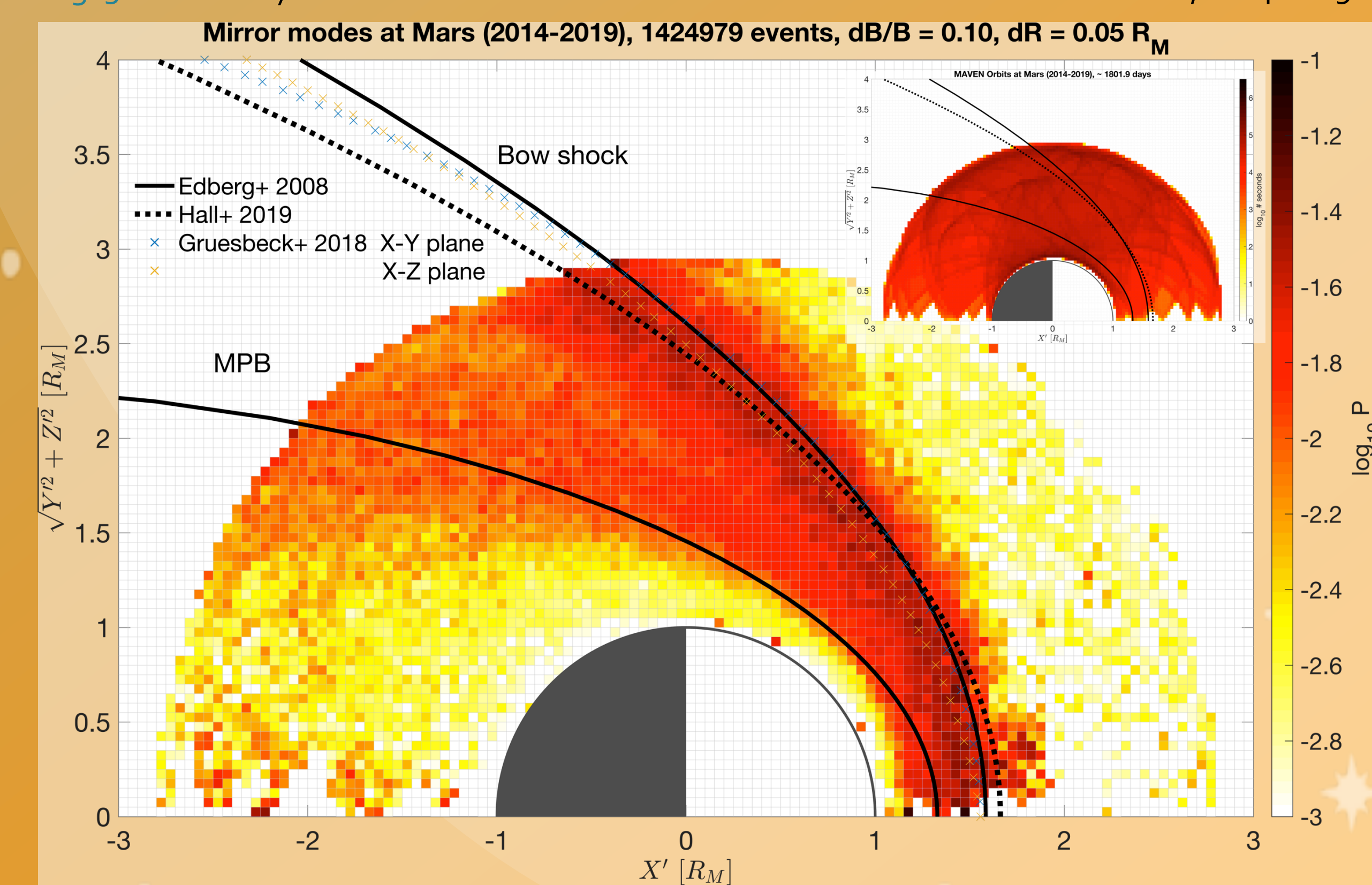
Mirror mode candidate detections are collected into a 2D axisymmetric grid in aberrated MSO coordinates, with a resolution of 0.05 Mars radius (Fig. 3). More than 10^6 events of 1 s are found for the whole 2014-2019 dataset. Maps are normalised by the spacecraft time of residence in each box (Fig. 3, top right), which shows an excellent coverage of a few 10s of hours on average per box (out of a total >1800 observation days, i.e., ~3 Martian years). Shock and magnetic pile-up (MPB) boundary models are shown for comparison.

The maximum occurrence probability P reaches about 10% (dark red) and is located close to the bow shock expected location. This is in visual agreement with Ruhunusiri+ (2015) for Mars and the beginning of MAVEN's survey, and with Volwerk+ (2016) for Venus.

Work currently in progress

- Use of the full instability criterion with SWIA/STATIC data to detect mirror mode waves, and hierarchical detection algorithm as in Song+ (1994).
 → Validation of B-field-only detection criteria
 - Evolution of occurrences vs Ls and solar activity
 - Determination of plasma β and shock conditions (quasi- \perp vs quasi- \parallel)
 - 3D characterisation of mirror mode occurrence rates
- Application to Mars and Venus datasets with the same magnetic field criteria

Fig. 3: Probability of occurrence of candidate mirror mode structures around Mars, 2014-2019.



Acknowledgements: CSW thanks F. Plaschke for suggestions. This work is supported by the Austrian Science Fund under FWF project P32035-N36.

Connerney, J. E. P., Espley, J., Lawton, P., et al. 2015, Space Sci. Rev., 195, 257, doi: 10.1007/s11214-015-0169-4
 Edberg, N. J. T., Lester, M., Cowley, S. W. H., & Eriksson, A. I. 2008, J. Geophys. Res., 113, n/a, doi: 10.1029/2008JA013096
 Gruesbeck, J. R., Espley, J. R., Connerney, J. E. P., et al. 2018, J. Geophys. Res., 123, 4542, doi: 10.1029/2018JA025366
 Halekas, J. S., Taylor, E. R., Dalton, G., et al. 2015, Space Sci. Rev., 195, 125, doi: 10.1007/s11214-013-0029-2
 Hall, B. E. S., Lester, M., Sánchez-Cano, B., et al. 2016, J. Geophys. Res., 121, 11,474, doi: 10.1002/2016JA023316
 Hall, B. E. S., Sánchez-Cano, B., Wild, J. A., Lester, M., & Holmström, M. 2019, J. Geophys. Res., 124, 4761, doi: 10.1029/2018JA026404
 Hasegawa, A. 1969, Phys. Fluids, 12, 2642, doi: 10.1063/1.1692107
 McFadden, J. P., Kortmann, O., Curtis, D., et al. 2015, Space Sci. Rev., 195, 199, doi: 10.1007/s11214-015-0175-6
 Ruhunusiri, S., Halekas, J. S., Connerney, J. E. P., et al. 2015, Geophys. Res. Lett., 42, 8917, doi: 10.1002/2015GL064968
 Song, P., Russell, C. T., & Gary, S. P. 1994, J. Geophys. Res., 99, 6011, doi: 10.1029/93JA03300
 Soucek, J., Lucek, E., & Dandouras, I. 2008, J. Geophys. Res., 113, doi: 10.1029/2007JA012649
 Volwerk, M., Zhang, T. L., Delva, M., et al. 2008, Geophys. Res. Lett., 35, n/a, doi: 10.1029/2008GL033621
 Volwerk, M., Schmid, D., Tsurutani, B. T., et al. 2016, Ann. Geophys., 34, 1099, doi: 10.5194/angeo-34-1099-2016